Molecular Therapy
Methods & Clinical Development
Original Article

Widespread correction of brain pathology in feline alpha-mannosidosis by dose escalation of intracisternal AAV vector injection

Jacqueline E. Hunter,[1] Caitlyn M. Molony,[2] Jessica H. Bagel,[2] Patricia O'Donnell,[2] Charles H. Vite,[2] Sanjeev Chawla,[3] Harish Poptani,[4] and John H. Wolfe[1,2,5]

[1]Research Institute of Children's Hospital of Philadelphia, Philadelphia, PA 19104, USA; [2]W.F. Goodman Center for Comparative Medical Genetics, School of Veterinary Medicine, University of Pennsylvania, Philadelphia, PA 19104, USA; [3]Department of Radiology, Perelman School of Medicine, University of Pennsylvania, Philadelphia, PA 19104, USA; [4]University of Liverpool, Liverpool L69 3BX, UK; [5]Department of Pediatrics, Perelman School of Medicine, University of Pennsylvania, Philadelphia, PA 19104, USA

Alpha-mannosidosis is caused by a genetic deficiency of lysosomal alpha-mannosidase, leading to the widespread presence of storage lesions in the brain and other tissues. Enzyme replacement therapy is available but is not approved for treating the CNS, since the enzyme does not penetrate the blood-brain barrier. However, intellectual disability is a major manifestation of the disease; thus, a complimentary treatment is needed. While enzyme replacement therapy into the brain is technically feasible, it requires ports and frequent administration over time that are difficult to manage medically. Infusion of adeno-associated viral vectors into the cerebrospinal fluid is an attractive route for broadly targeting brain cells. We demonstrate here the widespread post-symptomatic correction of the globally distributed storage lesions by infusion of a high dose of AAV1-feline alpha-mannosidase (fMANB) into the CSF via the cisterna magna in the gyrencephalic alpha-mannosidosis cat brain. Significant improvements in clinical parameters occurred, and widespread global correction was documented pre-mortem by non-invasive magnetic resonance imaging. Postmortem analysis demonstrated high levels of MANB activity and reversal of lysosomal storage lesions throughout the brain. Thus, CSF treatment by adeno-associated viral vector gene therapy appears to be a suitable complement to systemic enzyme replacement therapy to potentially treat the whole patient.

INTRODUCTION

Alpha-mannosidosis (AMD) is a lysosomal storage disease that occurs when lysosomal alpha-mannosidase is either absent or defective. It is estimated to occur in about 1 of 500,000 live births.[1] Clinical characteristics of AMD include hearing impairment, intellectual impairment, facial and skeletal abnormalities, hepatosplenomegaly, and immune deficiencies.[2] Many disease-causing mutations have been reported but with no apparent correlation between genotype and clinical phenotype.[1]

Current therapies for human AMD include hematopoietic stem cell transplantation (HSCT) and enzyme replacement therapy (ERT).[3] HSCT requires an appropriate donor and has a risk of graft versus host disease developing following treatment. Despite these limitations, there has been some success in AMD patients.[4] ERT is effective[5–7] and has been approved for human use in Europe and the US. However, it is not approved for treatment of the CNS disease, since the enzyme does not cross the blood-brain barrier (BBB). ERT also has several limitations. It requires weekly administration due to the short half-life of the enzyme; thus, there is a continuing high cost associated with treatment. The enzyme has limited effect on skeletal abnormalities, and it does not cross the BBB; thus, it is ineffective in treating the CNS. In principle, ERT could be used to treat the brain by injection into the cerebrospinal fluid (CSF), but that would require indwelling catheters for regular infusions, which are problematic to manage medically over long periods of time.

Adeno-associated viral (AAV) vector therapy is a promising alternative to current treatment methods for AMD and is potentially permanent. Injection into the CSF allows for direct targeting of the brain, with less vector available in circulation to trigger potential host responses. For diseases with a significant neurological component, this may allow for lower doses to be administered compared to systemic administration.[8] AAV delivery into the CSF can also allow targeting of the brain while evading circulating neutralizing antibodies.[8] To date, several clinical trials in other diseases have been conducted using CSF-directed routes of administration.[9,10]

Several naturally occurring AMD animal models exist, including cattle, cats, and guinea pigs.[11–13] A mouse AMD model has been generated;[14] however, this model has an attenuated AMD phenotype despite having a complete absence of alpha-mannosidase (MANB)

Received 13 December 2023; accepted 20 May 2024;
https://doi.org/10.1016/j.omtm.2024.101272.

Correspondence: John H. Wolfe, Children's Hospital of Philadelphia, 502-G Abramson Research Center, 3615 Civic Center Boulevard, Philadelphia, PA 19104-4399, USA.
E-mail: jhwolfe@vet.upenn.edu

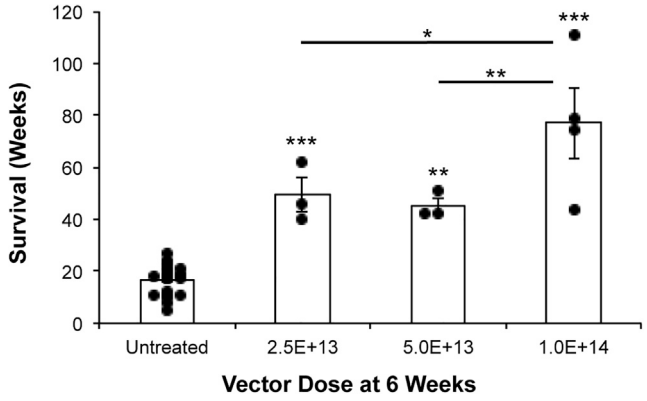

Figure 1. Survival of AAV1-fMANB-treated AMD cats increases in a dose-dependent manner

AMD cats were treated at 6 weeks of age with a single intracisternal injection of AAV1 expressing fMANB at a dose of 2.5×10^{13} vg ($n = 3$), 5.0×10^{13} vg ($n = 3$), or 1.0×10^{14} vg ($n = 4$). Treated cats lived longer than untreated cats, with mean survival increasing with vector dose. Error bars represent mean +SEM. $^{*}p < 0.05$, $^{**}p < 0.01$, $^{***}p < 0.001$.

activity. The cat brain is closer in size to the human brain than the rodent brain, and the gyrencephalic brain structure results in circuits and pathways that are similar to the primate brain.[15] The cat is a well-established model for neurological studies, and AMD in the cat shows heterogeneity in disease similar to what is observed in human patients.[16]

The AMD cat model has been used for HSCT[17] and gene therapy experiments.[18–20] AAV1 has been shown to have superior transduction of the cat brain compared to AAV9, a serotype widely used for CNS transduction.[19] A comparison of several other serotypes demonstrated that AAV1 mediates broader distribution and levels of transduction, with only the very closely related AAV6 being similar.[21] AAV1 is also capable of transducing both choroid plexus and ependymal cells.[21] Transduction of these cell types may allow for production and secretion of therapeutic enzyme that is pumped into CSF circulation, potentially allowing for greater distribution within the CNS.[22] A previous study showed that a single injection of AAV1 into the CSF of AMD cats could mediate partial improvement in the clinical disease, but treatment was incomplete.[19] The current study demonstrates that high vector doses delivered via the cisterna magna (cm) result in significant reductions and, in many areas, complete reversal of storage lesions throughout the AMD cat brain.

RESULTS

Clinical improvement is dose dependent in CM-treated AMD cats

The average lifespan of an untreated AMD cat is 16.2 ± 1.7 weeks.[18,19,23] We previously observed a significant increase in survival of animals injected intracisternally at 6 weeks of age with 1.0×10^{13} vector genomes (vg) AAV1- fMANB, which encodes fMANB under the control of the human beta-glucuronidase promoter.[19] Three escalating doses of AAV1-fMANB (2.5×10^{13}, 5×10^{13}, and 1.0×10^{14} vg) were tested to determine whether lifespan could be further lengthened. Animals were injected intracisternally at 6 weeks of age, as this is after the age at which clinical symptoms being to appear in the AMD cat.[18] Increasing the vector dose provided a subsequent increase in survival (Figure 1), with some individuals in the higher-dose groups surviving to more than 1 year of age (mean survival 49.3 ± 6.6 weeks for the 2.5×10^{13} vg group, 45.3 ± 2.8 weeks for the 5.0×10^{13} vg group, and 77.0 ± 15.8 weeks for the 1.0×10^{14} vg group).

In untreated AMD cats, tremors and truncal ataxia develop by 8 weeks of age.[18,19] Neurological exams identified mild tremors occurring in 2 of 3 animals in the 2.5×10^{13} vg dose group. Tremors did not occur before the humane endpoint in 2 of 3 cats in the 5×10^{13} vg group and 3 of 4 cats in the 1×10^{14} vg group. Ataxia was observed at 17 weeks of age for one cat in the 2.5×10^{13} vg group, and intermittent ataxia was observed at 20 weeks of age for one cat in the 5×10^{13} vg group. One animal each of the 2.5×10^{13} vg and 5×10^{13} vg groups was non-ataxic but developed a waddling gait. Due to the COVID-19 pandemic, it was not possible to regularly perform neurological exams; therefore, the precise age at which tremors and ataxia developed could not be determined for all treated animals.

CSF and serum samples were collected before injections and at regular intervals post injection. MANB enzymatic activity was calculated as the percent activity of normal cat CSF or serum samples (% normal). At a dose of 1.0×10^{13} vg AAV1-fMANB, MANB activity in the CSF was significantly above that of untreated animals for the first 1–3 months post injection; however, this difference was no longer statistically significant from 4 to 6 months post injection.[19] We tested total doses of 2.5×10^{13}, 5×10^{13}, and 1.0×10^{14} vg. All 3 doses produced significantly higher fMANB activity levels in the CSF compared to both untreated and the 1.0×10^{13} vg dose, and the MANB enzymatic activity remained elevated over time (Figure 2A). The 1.0×10^{14} vg dose resulted in a sharp increase in enzyme activity (35% of normal) for the first 1–2 months post injection that then decreased over time but did not decrease below 10% of normal. MANB activity in serum was also elevated above that of untreated cats (Figure 2B); however, the increase was not as high as observed in the CSF. Furthermore, the serum MANB activity in the cats treated with higher doses did not exceed that observed in cats treated with the low dose reported previously.[19]

MANB enzymatic activity in the treated AMD brain

Treated AMD cats were euthanized upon reaching the humane endpoint. To measure fMANB enzymatic activity in the brain, coronal sections at different intervals along the rostral-caudal axis were analyzed (Figure S1A).[19,20] MANB enzymatic activity was calculated as the percent activity of normal cat brain sections (% normal). A dose-dependent increase in MANB activity was observed, with all doses generating an increase in enzymatic activity over that seen in untreated AMD cats (Table 1). The coefficient of determination (R2) between MANB activity and longevity was statistically significant (R2 = 0.4958, $p < 0.05$).

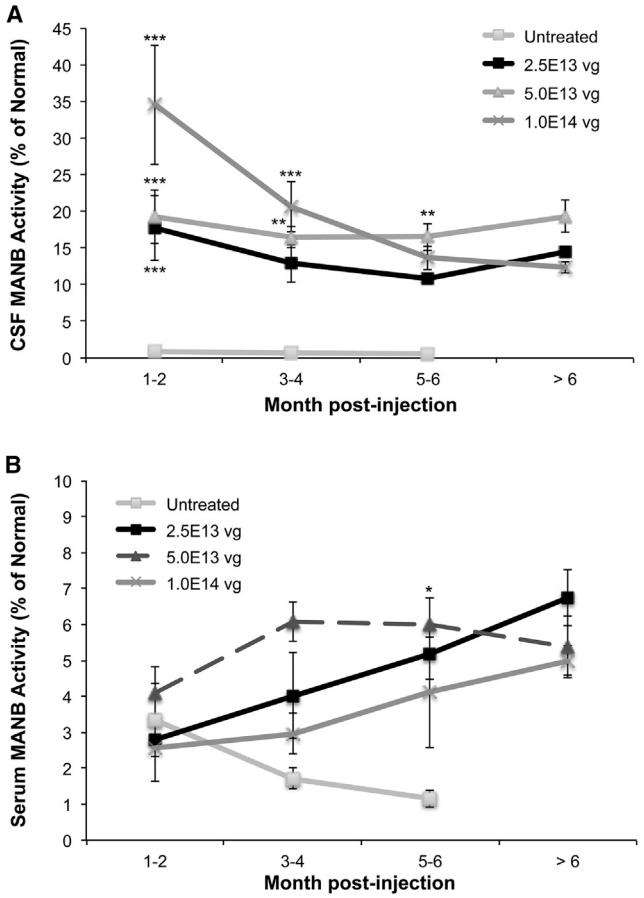

Figure 2. MANB activity is elevated in CSF, but not serum, of treated AMD cats

CSF and serum samples were collected at regular intervals and assayed for MANB activity in both treated and untreated AMD cats. (A) CSF MANB activity was significantly higher than in untreated cats up to 6 months post injection. (B) Serum MANB activity was comparable to untreated cats for the first 1–2 months post injection but increased over time. There was no significant difference between dose groups. Note that comparisons to untreated cats cannot be made at time points greater than 6 months post injection as untreated cats do not live that long. Points represent mean + SEM. $^{*}p < 0.05$, $^{**}p < 0.01$, $^{***}p < 0.001$.

The number of vector genome copies were also assayed from coronal sections collected at different intervals along the rostral-caudal axis (Figure S1B). While the vector genome copies detected were generally low, there was a small increase in most hemisections for the highest-dose group (Table 2). Taken together, the data demonstrate that CM administration of AAV1-fMANB leads to widespread distribution of the fMANB cDNA throughout the brain, and MANB enzymatic activity throughout the brain increases in a dose-dependent manner.

Correction of lysosomal storage lesions in treated AMD cat brains

The hallmark of AMD is the accumulation of undegraded substrate in lysosomes, resulting in distended storage vacuoles in cells throughout the body. To determine whether the increase in MANB enzymatic activity translates to a decrease in the presence of lysosomal storage vacuoles, histology was performed on brain sections taken from multiple sites along the rostral-caudal axis. In the brain, this storage can be visualized by H&E-stained sections. Increasing the vector dose allowed for more correction of storage vacuoles (Figure 3), with the amount of correction observed in the two highest-dose groups being similar and indistinguishable from normal.

Another hallmark of AMD that can be visualized histologically is the demyelination of white matter tracts. Luxol fast blue-stained sections from untreated cats showed decreased intensity of staining as well as distension and splitting of the myelin sheaths in white matter when compared with normal animals.[23] Treatment improved the appearance of the white matter in the centrum semiovale, internal capsule, and cerebellar white matter (Figure 4), with the myelin from animals in the higher-dose groups being similar in appearance to that of normal cats.

Magnetic resonance spectroscopy and diffusion tensor imaging show reduction of storage at high doses

Monitoring changes in the AMD brain by non-invasive imaging during the course of treatment can be accomplished by magnetic resonance spectroscopy (MRS) and diffusion tensor imaging (DTI).[24–26] The most sensitive measure of brain correction is MRS, which is a direct measure of the undegraded oligosaccharides in the brain.[20] Both the 5.0×10^{13} and 1.0×10^{14} vg doses mediated reduction of the oligosaccharide peaks to the levels measured in the normal cat brain (Table 3). DTI can assess the changes in white matter tracks, which are extensively altered in AMD and partially corrected at the two highest doses (Table 3).

The cats were imaged at approximately 4-month intervals during the study. The concordance of reduction in the mannose-rich oligosaccharide peak centered at 3.8 ppm[25] down to normal was maintained over time in each dose group. Traces across time for a representative cat in each dose group are shown in Figure S2.

Transduction and correction of lesions in non-CNS organs of treated AMD cats

Delivering therapeutic protein to the CSF may also lead to a small amount of the protein passing into the periphery, as seen in a study of canine Batten disease.[27] In the AMD cats treated at 6 weeks of age, MANB activity was measured in the liver, kidneys, heart, and spleen. No significant change was detected for any dose in any of the other organs tested (Table S1). Vector genome copies were variable but low in all samples evaluated (Table S2).

In order to evaluate potential vector-induced toxicity, serum chemistry was evaluated from treated cats. Markers for liver and kidney function were elevated in several of the cats (Table S3); however, it is unclear whether this is due to vector treatment or disease induced. H&E-stained liver sections from treated cats appeared similar to those from untreated cats, with storage present in cells throughout the

Table 1. MANB activity measured in multiple brain hemisections along the rostral-to-caudal axis

		Hemisection					
Treatment group	Animal	1	2	3	4	5	6
Untreated	1	1.065	0.591	0.630	1.210	0.806	0.739
	2	0.519	0.372	0.437	0.585	0.793	0.800
	3	0.631	0.704	0.779	0.957	0.958	0.745
	4	0.528	0.626	0.743	0.684	1.111	0.901
	Average (+ SEM)	0.686 (0.129)	0.573 (0.071)	0.647 (0.077)	0.859 (0.141)	0.917 (0.075)	0.796 (0.037)
2.5×10^{13} vg	1	3.405	3.580	3.998	5.176	5.796	8.347
	2	4.692	5.793	4.888	7.714	7.485	5.700
	3	4.558	4.892	4.540	6.354	6.252	5.847
	Average (+ SEM)	4.218 (0.409)	4.755 (0.642)	4.475 (0.259)	6.415 (0.733)	6.511 (0.504)	6.631 (0.859)
$5.0E \times 10^{13}$ vg	1	6.584	6.741	14.823	24.482	17.628	15.910
	2	4.011	4.257	3.715	6.815	3.425	5.687
	3	6.716	7.029	7.600	10.823	4.257	8.689
	Average (+ SEM)	5.770 (0.881)	6.009 (0.880)	8.713 (3.254)	14.040 (5.348)	8.437 (4.602)	10.095 (3.034)**
1.0×10^{14} vg	1	5.064	5.949	6.088	9.944	10.067	9.272
	2	14.916	14.020	13.758	22.442	22.801	13.066
	3	13.157	11.401	10.292	15.521	14.664	6.866
	4	18.718	15.419	16.852	25.295	22.529	10.296
	Average (+ SEM)	12.963 (2.877)**,+	11.697 (2.089)***,+	11.747 (2.314)**	18.301 (3.460)**	17.515 (3.118)**	9.875 (1.284)**

Brain fMANB activity in both treated and untreated AMD cats was measured in coronal sections taken at regular intervals along the rostral-caudal axis. Activity is calculated and reported as a percentage of normal. $^{**}p < 0.01$, $^{***}p < 0.001$ compared to untreated animals. $+p < 0.05$ compared to the 2.5×10^{13} vg group.

tissue (Figure S3). There did not appear to be any significant increase in immune cell infiltrate in any of the sections analyzed.

DISCUSSION

Intracisternal (CM) delivery is a clinically relevant route of administration that provides several benefits over other routes. Delivery of AAV vector to the CM allows efficient targeting of the brain that is less invasive than direct brain injection. While systemic delivery is easier to perform clinically, it does not provide for specific delivery to the CNS, which may lead to off-target expression of the therapeutic gene and potentially a greater risk of vector- or transgene-induced toxicity. The CM delivery route is not commonly used in clinical practice due to the risk of damage to the brain stem or vascular structures. The concern of potential risks of injection into the human CM is solved by passing a microcatheter from the lumbar cistern up into the CM,[28] which has been used clinically to treat human Tay-Sachs disease.[10] The critical issue for animal experiments is to deliver the vector into the CM, not how to access the CM for the infusion.

A 1.0×10^{13} vg dose resulted in some clinical improvement in the AMD cat; however, the histologic correction of storage lesions was partial.[19] The current study indicates that therapeutic response in AMD cats increases with dose, as demonstrated by significant increases in survival, MANB activity in the brain, and resolution of lysosomal storage in brain sections.

The 2.5×10^{13} vg dose in the present study resulted in some clinical improvement over the 1.0×10^{13} vg dose, but the correction of storage lesions was still incomplete. For the 5.0×10^{13} and 1.0×10^{14} vg treatment groups, there was a significant reduction of lysosomal storage and a near-normal appearance of gray matter and myelin. The MRS results indicate that the reduction in storage was similar to normal at each of the higher doses. The brain size at the initiation of treatment at 6 weeks in the cat (~20 gram) is approximately proportional to a 1-year-old child's brain (~800 gram). Thus, a dose of 5.0×10^{13} in the cat would translate to a dose of $\sim 2.0 \times 10^{15}$ vg in a human brain of equivalent age. For translational consideration, the dose used is per brain, and human brain size reaches ~90% of the adult size at about 5 years of age; thus, the increase in the effective dose for CSF treatment would be relatively small after that. In contrast, the dose required for significant brain correction by systemic gene delivery that crosses the BBB is based on body weight;[9] thus, treatment of most patients would require a larger total dose than by CSF delivery.

While survival and brain MANB activity increased with dose, it is unclear why the highest dose afforded a longer average survival over the 5.0×10^{13} vg dose despite comparable reduction of lysosomal storage and similar appearance of gray matter and myelin between the two groups. It is possible that, in the highest-dose group, a greater amount of fMANB enzyme is transported to the periphery. However, this possibility is not reflected in the postmortem enzyme activity in multiple

Table 2. AAV1-fMANB vector genome copies measured in multiple brain hemisections along the rostral-to-caudal axis

		Hemisection					
Treatment group	Animal	1	2	3	4	5	6
2.5×10^{13} vg	1	6.554	1.086	3.796	1.333	3.106	1.659
	2	1.775	1.471	6.252	3.450	3.608	2.617
	3	6.539	2.464	4.214	3.431	9.879	1.814
	Average (+ SEM)	4.956 (1.590)	1.674 (0.411)	4.754 (0.759)	2.738 (0.703)	5.531 (2.179)	2.030 (0.297)
5.0×10^{13} vg	1	5.743	3.074	18.761	9.285	8.364	5.118
	2	0.480	0.095	0.107	0.143	0.050	0.044
	3	0.480	0.437	0.388	0.189	0.329	0.326
	Average (+ SEM)	2.234 (1.754)	1.202 (0.941)	6.418 (6.172)	3.206 (3.040)	2.915 (2.726)	1.829 (1.647)
1.0×10^{14} vg	1	0.168	0.183	0.387	0.322	0.194	0.057
	2	31.925	7.204	9.698	8.587	9.763	2.272
	3	39.041	11.914	17.100	5.968	7.786	1.623
	4	15.247	11.642	10.133	11.492	3.991	1.576
	Average (+ SEM)	21.595 (8.711)	7.736 (2.739)	9.330 (3.429)	6.592 (2.375)	5.433 (2.118)	1.382 (0.469)

AAV1-fMANB vector genome copies in treated AMD cats were measured in coronal sections taken at regular intervals along the rostral-caudal axis. Data are calculated and reported as copies per diploid genome.

organs or in the routine serum samples taken during the life of the animal. It is important to note that the therapeutic enzyme in this and other lysosomal storage diseases is being continuously consumed metabolically by the normal lysosomal degradation pathways.[29,30]

While AAVs are generally non-pathogenic, it is possible that the highest dose used in this study (1×10^{14} vg) may be sufficient to trigger an adverse response, hampering therapeutic benefit.[31] We did not observe any evidence of vector-induced toxicity in brain sections analyzed for this study. While some animals had an increase in liver enzymes or markers of kidney function (Table S3), the increase was not consistent within a dose group. Furthermore, these abnormalities could be a consequence of disease progression in these tissues. Histological evaluation of liver tissue samples taken from treated animals contained storage lesions similar to those of untreated animals (Figure S3).

The lack of toxicity observed in this study may be attributed to the choice of promoter and transgene used. As AMD is present in all tissues, we opted to use the human GUSB promoter due to its ability to drive moderate expression in all tissues.[32] Its small size also allows for the packaging of larger genes, such as fMANB (3-kb coding sequence), into an AAV backbone. Other ubiquitous promoters, such as CMV and CBA, have been successful in driving high transgene expression in other studies, but it comes with a risk of toxicity due to high levels of transgene expression. When compared to neuron-specific CaMKII and SynI promoters, CMV-driven GFP expression was correlated with a toxic effect on neurons and infiltration of glia cells in the marmoset brain.[33] We also opted to use the feline MANB cDNA in our studies, instead of human MANB, to reduce the risk of generating an immune response to non-self protein.

Another area of interest currently is the incidence of dorsal root ganglion (DRG) toxicity following AAV vector administration. DRG lesions were initially observed following intravascular delivery of AAVhu68-hSMN to non-human primates (NHPs) and piglets.[34] Lesions were not present in all DRGs but, when present, consisted of neuronal degeneration, increased cellularity, and nerve fiber degeneration. While the lesions were clinically silent in the NHPs, piglets in this study developed proprioceptive deficits and ataxia. Other studies using different vectors and routes of administration also observed DRG lesions in NHPs; however, it was noted that the lesions did not translate into sensory deficits in the animals.[35,36] Dose-dependent DRG lesions have also been observed in rats and mice.[36,37] The mechanism of DRG toxicity it not well understood at this time; however, continuing research into the nature of the AAV-induced DRG toxicity suggests that it may be species specific[38] and/or a result of high levels of transgene expression.[36,38,39] Although we were unable to assess whether DRG toxicity is present in the animals in this study, since DRGs were not collected from all animals, a meta-analysis of all available studies in DRG pathology found a notable absence of any clinical sequelae while using therapeutic transgenes.[38]

Future studies will investigate whether age at treatment has any effect on clinical response. The AMD cat begins to show clinical signs of disease at 5 weeks of age; therefore, it will be of interest whether treatment at earlier (pre-symptomatic) or later (post-symptomatic with progressive disease) has significant effects on clinical outcome, with the dose adjusted for relative brain growth at different ages. As MANB ERT is currently available for AMD patients, it would also be of interest whether the combination of ERT and intracisternal vector delivery would produce additional improvements of clinical outcomes.

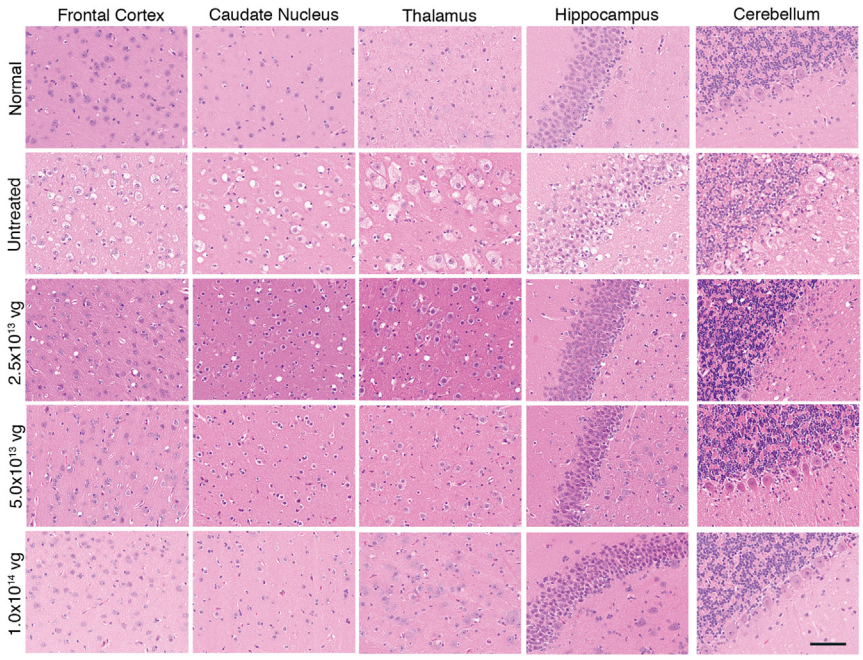

Figure 3. Clearance of lysosomal storage lesions in the brain is dose dependent

Representative H&E-stained brain sections of normal, untreated, and AAV1-fMANB-treated cats. Partial storage reduction is seen in the 2.5×10^{13} vg dose group, with the two higher doses producing near-complete correction. Scale bar, 100 μm.

MATERIALS AND METHODS

Plasmid and AAV production

The gene transfer *cis*-plasmid containing the fMANB gene was expressed from the minimal human GUSB promoter in the pZac vector that included an SV40 splice donor/acceptor signal and the bovine growth hormone polyadenylation signal, as described.[32,40–42] Recombinant AAV1 vectors were packaged by the University of Pennsylvania Vector Core by triple transfection of HEK293 cells with the AAV *cis*-plasmid, AAV *trans*-plasmid containing AAV rep and cap genes, and adenovirus helper plasmid. Vectors were purified using iodixanol gradient ultracentrifugation, and the titers were determined by real-time PCR.[43]

To achieve precise differences in the treatment dose, the vectors from multiple megapreps were combined and concentrated by size exclusion to $>1.0 \times 10^{14}$ genome copies (gc)/mL, the maximum dose to be tested. The maximum volume of vector that can be injected into the cisterna magna of a kitten at one time is 1 mL. The pooled vector was re-titered in triplicate independent assays. The stock was divided into exact dilutions by volume to ensure precise increments of 10×, 5×, and 2.5× doses, and each stock was divided into individual aliquots of 1 mL and stored at −80°C for injection into a single animal. This ensured that all animals within a dose received exactly the same amount of vector and that the doses were exactly double the next-lower dose (i.e., 2.5, 5.0, and 10.0×10^{13} vg).

Animals and vector injections

All animal care and procedures were performed in accordance with the Institutional Animal Care and Use Committee at the University of Pennsylvania. AMD-affected cats were produced in the breeding colony of the University of Pennsylvania School of Veterinary Medicine by carrier-to-carrier breeding. At 6 weeks of age, cats were anesthetized with intravenous (i.v.) propofol (up to 6 mg/kg). A catheter was placed in the cephalic vein, and enough propofol was given to allow intubation. Animals were positioned in right-side lateral recumbency and were anesthetized during the procedure. Using sterile techniques, approximately 0.5 mL of CSF was collected using a 22G needle from the cerebellomedullary cistern. After collecting CSF, AAV1-fMANB was injected over the course of 1 min with a dwell time of approximately 5 s. The injected dose in cats was 2.5×10^{13} vg, 5.0×10^{13} vg, or 1.0×10^{14} vg. Heart and respiratory rates were monitored until full recovery. All of the animals were injected at the same age, by the same staff, and using the same procedure. The surgeon and vivarium staff were all blind to the dose received. Animals were assessed daily by veterinarians or trained veterinary staff and were euthanized when they reached the humane endpoint. Criteria for euthanasia included (1) loss of 15% of body weight, (2) loss of responsiveness to human interaction, and (3) significant changes in behavior or attitude relative to what is normal monthly from treatment until euthanasia by the same blind observer who was unaware of whether cats were treated or not. The onset and progression as well as the severity of signs of neurologic dysfunction were identified. However, due to the COVID-19 pandemic, it was not possible to perform neurological exams regularly; therefore, the precise age at which tremors and ataxia developed could not be determined for all treated animals.

MANB enzymatic activity assay

MANB enzymatic activity was measured in serum, CSF, or brain tissue as described.[18–20] Tissues were homogenized in saline containing 0.2% Triton X-100, and MANB activity was determined using the substrate 4-methylumbelliferyl α-D-mannopyranoside in 0.1 M sodium citrate buffer (pH 4.4) at 37°C for 1 h. Protein was quantified using bicinchoninic acid assay.

Tissue collection and preparation

Treated cats were allowed to live as long as possible and were euthanized when humane endpoint criteria were reached according to the IACUC protocol. Euthanasia was performed using an overdose of i.v. barbiturates transcardially perfused with 0.9% cold saline. Tissues were drop fixed in 4% paraformaldehyde for 48 h. Euthanasia allowed

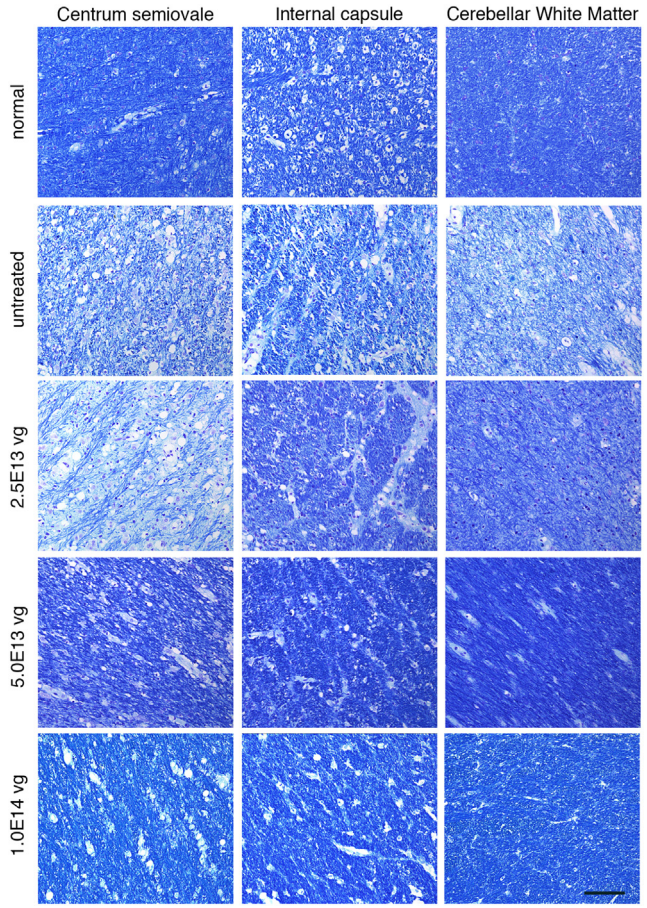

Figure 4. Normalization of white matter regions is dose dependent
Representative Luxol fast blue-stained brain sections of normal, untreated, and AAV1-fMANB-treated cats. Partial improvement of myelin intensity is seen in the 2.5×10^{13} vg dose group, with the two higher doses producing near-complete normalization. Scale bar, 100 μm.

these brains to be perfused with PBS and immediately transferred to paraformaldehyde in order to preserve brain morphology.

For cryosectioning, brains were cryoprotected in 30% sucrose, embedded in optimum cutting temperature solution (Sakura, Torrance, CA, USA), and cryosectioned at 40 μm (Leica Microsystems, Wetzlar, Germany). For histology, tissues were paraffin embedded and stained with H&E or Luxol fast blue.

For serum collection, whole blood was allowed to clot for 30 min at room temperature and then centrifuged at 1,000 × *g* for 15 min. The supernatant was then aspirated and stored at −80°C. CSF was collected using a 22G spinal needle from the cerebellomedullary cistern and stored at −80°C.

Real-time PCR

Quantitative real-time PCR was used to determine the viral genome copies present in the brain. Genomic DNA was extracted from 2–3 sections of each transverse brain block, and the vector genome copies were quantified separately at each transverse level. Copies of fMANB vector genome were quantified using PowerUp SYBR Green Master Mix (Thermo Fisher, Austin, TX, USA). Triplicate samples derived from each DNA pool were used for quantification. The fMANB primer sequences were as follows: forward, 5′-GGG AGG AGC ATG GCT AGA CA-3′; reverse, 5′-AAC AAC AGA TGG CTG GCA ACT-3′.

MRI

All cats underwent MRI on a 3T Tim Trio whole-body magnetic resonance scanner (Siemens) equipped with a single-channel 11-cm internal diameter transmit-receive birdcage coil (M2M). The anatomical imaging protocol included a 3-plane scout localizer to determine the orientation and position of the brain. Additionally, axial T2-weighted images (repetition time/echo time = 2,500/60 ms); section thickness = 2 mm; number of slices = 20; number of excitations = 1; and axial T1-weighted images (repetition time/echo time = 650/27 ms) were acquired. Physiological monitoring, including pulse oximetry and vital signs (oxygen saturation and heart rate), was recorded before and during the entire scanning period.

Proton MRS imaging

Single-slice 2D multivoxel proton MRS imaging (^{1}H-MRS) was performed using a spin echo (point-resolved spectroscopy) sequence with water suppression using a chemical shift selective saturation sequence. Sequence parameters included repetition time/echo time (2,500/30 ms), number of excitations (16), field of view (55 × 55 mm^2), slice thickness (7 mm), bandwidth (1,500 Hz), and matrix size (16 × 16). The typical voxel size was 3.4 × 3.4 × 7 mm^3. The volume of interest was selected to include the different cortical and thalamic regions, avoiding the scalp. Four outer volume saturation slabs (30 mm thick) were placed outside the volume of interest to suppress Lip signals from the scalp. The dataset was acquired using elliptical k-space sampling with weighted phase encoding to reduce the acquisition time. Acquisition time for the ^{1}H-MRS sequence was 6:22 min. Manual shimming was performed to achieve an optimal value of full width half-maximum of the water signal. In general, a shimming of 520 Hz was achieved on the magnitude signal of the water resonance. Water unsuppressed ^{1}H-MRS spectra were also acquired to use the water signal for computing relative metabolite ratios.

DTI

DTI data were acquired using 30 non-collinear/non-coplanar directions with a single-shot spin echo, echo-planar readout sequence. The sequence parameters were as follows: repetition time/echo time = 3,000/75 ms; number of excitations = 8; field of view = 80 × 80 mm^2; matrix size = 64 × 64; in-plane resolution = 1.25 × 1.25 mm^2; slice thickness = 2 mm; b = 0, 1,000 s/mm^2; and number of slices = 20, covering the whole brain.

Table 3. MR spectroscopy and DTI from AAV CSF-treated cats at 3 doses

				MRS Ms/H_2O ratio ($\times 10^{-3}$)		DTI FA		
Genotype	Vector	Titer	*n*	Cerebral cortex	Thalamus	External capsule	Internal capsule	Corpus callosum
Normal	none	N/A	3	0.14 (0.06)	0.13 (0.05)	0.66 (0.05)	0.68 (0.05)	0.29 (0.04)
AMD	none	N/A	5	1.96 (0.30)	2.11 (0.31)	0.44 (0.02)	0.46 (0.07)	0.22 (0.02)
AMD treated	AAV1- fMANB	2.5 × 10e13	3	1.68 (0.11)	1.69 (0.09)	0.51* (0.04)	0.46 (0.06)	0.25 (0.02)
AMD treated	AAV1- fMANB	5.0 × 10e13	3	0.20**** (0.04)	0.17**** (0.02)	0.57*** (0.02)	0.58* (0.06)	0.27* (0.02)
AMD treated	AAV1- fMANB	1.0 × 10e14	5	0.18**** (0.03)	0.17**** (0.02)	0.52** (0.03)	0.55* (0.03)	0.27** (0.01)

MRS is expressed as ratios of areas under the curve (integration) of metabolites to water for the mannose-rich (ms) oligosaccharide peaks (±SD) as shown in Magnitsky et al.[25] The DTI measure used is FA (±SD), as shown in Kumar et al.[24] *$p \leq 0.05$, **$p < 0.01$, ***$p < 0.001$, ****$p < 0.0001$. Treated cats were compared to untreated AMD cats using a t test.

Data analysis

The ^{1}H-MRS data were processed offline on a Leonardo workstation using the Syngo software (Siemens). For each spectrum, the acquired ^{1}H-MRS signal (free induction decay) was zero filled (2,048 datapoints), smoothed (Hanning filter; width, 200 ms), and Fourier transformed. This was followed by phase (zero- and first-order polynomial) and baseline correction for optimal linear frequency dependence. Peak areas of oligosaccharide (3.4–3.9 ppm) and unsuppressed water (4.8 ppm) resonances were determined from each voxel encompassing the bilateral cortical and thalamic regions. The fitting of the individual peak can be optimized by adjusting the chemical shift, amplitude, and line width interactively. Peak areas of oligosaccharide were normalized with respect to the unsuppressed water signal for each voxel. The metabolite ratios for oligosaccharide/water from 5 to 10 voxels that encompassed the cortex and four to six voxels that encompassed the thalamus were computed. The mean and SD values of metabolite ratios of oligosaccharide/water were reported from each region.

DTI data were processed and analyzed using DTI studio software (Johns Hopkins School of Medicine; www.mristudio.org). Pixel-wise fractional anisotropy (FA) maps were computed. FA color maps were used to draw the regions of interest from white matter regions (corpus callosum, external and internal capsule). These regions of interest were translated on FA maps to compute FA values, since FA was the only *in vivo* DTI parameter at 3 T that statistically distinguished normal from untreated AMD brains.[24]

Statistical analysis

Unpaired two-tailed Student's t test and one-way ANOVA with Bonferroni post-test were used, where applicable, to determine mean differences between groups. Data are reported as means ± SEM unless otherwise stated. For the imaging studies, the ^{1}H-MRS data metabolite ratios of oligosaccharide/water from cortical and thalamic regions were compared across different groups of animals (normal, untreated AMD, 2.5 × 10^{13} vg treatment, 5.0 × 10^{13} vg treatment, and 1.0 × 10^{14} vg treatment) by one-way ANOVA with a post hoc Bonferroni test. Similarly, FA values as obtained from DTI data from the corpus callosum, external capsule, and internal capsule were compared across different groups of animals. All data analyses were performed using a statistical tool (SPSS for Windows, v.18.0; SPSS, Chicago, IL, USA).

DATA AND CODE AVAILABILITY

All data and supporting materials are available within the article and supplemental information. Raw data can be provided by the corresponding author upon reasonable request.

SUPPLEMENTAL INFORMATION

Supplemental information can be found online at https://doi.org/10.1016/j.omtm.2024.101272.

ACKNOWLEDGMENTS

We thank A. Polesky for expert technical assistance and S.N. Ashley for vector preparation advice. This work was supported by NIH grant R01-NS110349 to J.H.W.

AUTHOR CONTRIBUTIONS

J.E.H. and J.H.W. designed the experiments. C.M.M., J.H.B., C.H.V., and P.O. performed injections and provided medical management. J.H. performed enzyme activity and PCR experiments. S.C. and H.P. performed MRS and DTI procedures and data analyses. J.E.H. and J.H.W. analyzed the data and wrote the manuscript.

DECLARATION OF INTERESTS

The authors declare no competing interests.

REFERENCES

1. Malm, D., and Nilssen, Ø. (2008). Alpha-mannosidosis. Orphanet J. Rare Dis. *3*, 21.
2. Malm, D., Riise Stensland, H.M.F., Edvardsen, Ø., and Nilssen, Ø. (2014). The natural course and complications of alpha-mannosidosis—a retrospective and descriptive study. J. Inherit. Metab. Dis. *37*, 79–82.
3. Wolfe, J.H. (2024). Disorders of glycoprotein degradation: α-mannosidosis, β- mannosidosis, fucosidosis, sialidosis, and aspartylglycosaminuria. In Rosenberg's Molecular and Genetic Basis of Neurological and Psychiatric Disease, 7th Edition, *vol 1*, R.N. Rosenberg and J.M. Pascual, eds. (Elsevier).

4. Ceccarini, M.R., Codini, M., Conte, C., Patria, F., Cataldi, S., Bertelli, M., Albi, E., and Beccari, T. (2018). Alpha-Mannosidosis: Therapeutic Strategies. Int. J. Mol. Sci. *19*, 1500.

5. Borgwardt, L., Guffon, N., Amraoui, Y., Dali, C.I., De Meirleir, L., Gil-Campos, M., Heron, B., Geraci, S., Ardigò, D., Cattaneo, F., et al. (2018). Efficacy and safety of Velmanase alfa in the treatment of patients with alpha-mannosidosis: results from the core and extension phase analysis of a phase III multicentre, double-blind, randomised, placebo-controlled trial. J. Inherit. Metab. Dis. *41*, 1215–1223.

6. Roces, D.P., Lüllmann-Rauch, R., Peng, J., Balducci, C., Andersson, C., Tollersrud, O., Fogh, J., Orlacchio, A., Beccari, T., Saftig, P., and von Figura, K. (2004). Efficacy of enzyme replacement therapy in α-mannosidosis mice: a preclinical animal study. Hum. Mol. Genet. *13*, 1979–1988.

7. Santoro, L., Zampini, L., Padella, L., Monachesi, C., Zampieri, S., Dardis, A., Cordiali, R., Galeazzi, T., and Catassi, C. (2020). Early biochemical effects of velmanase alfa in a 7-month old infant with alpha-mannosidosis. JIMD Rep. *55*, 15–21.

8. Gray, S.J., Nagabhushan Kalburgi, S., McCown, T.J., and Jude Samulski, R. (2013). Global CNS gene delivery and evasion of anti-AAV-neutralizing antibodies by intrathecal AAV administration in non-human primates. Gene Ther. *20*, 450–459.

9. Chen, X., Lim, D.A., Lawlor, M.W., Dimmock, D., Vite, C.H., Lester, T., Tavakkoli, F., Sadhu, C., Prasad, S., and Gray, S.J. (2023). Biodistribution of Adeno-Associated Virus Gene Therapy Following Cerebrospinal Fluid-Directed Administration. Hum. Gene Ther. *34*, 94–111.

10. Flotte, T.R., Cataltepe, O., Puri, A., Batista, A.R., Moser, R., McKenna-Yasek, D., Douthwright, C., Gernoux, G., Blackwood, M., Mueller, C., et al. (2022). AAV gene therapy for Tay-Sachs disease. Nat. Med. *28*, 251–259.

11. Burditt, L.J., Chotai, K., Hirani, S., Nugent, P.G., Winchester, B.G., and Blakemore, W.F. (1980). Biochemical studies on a case of feline mannosidosis. Biochem. J. *189*, 467–473.

12. Crawley, A.C., and Walkley, S.U. (2007). Developmental analysis of CNS pathology in the lysosomal storage disease alpha-mannosidosis. J. Neuropathol. Exp. Neurol. *66*, 687–697.

13. Hocking, J.D., Jolly, R.D., and Batt, R.D. (1972). Deficiency of alpha-mannosidase in Angus cattle. An inherited lysosomal storage disease. Biochem. J. *128*, 69–78.

14. Stinchi, S., Lüllmann-Rauch, R., Hartmann, D., Coenen, R., Beccari, T., Orlacchio, A., von Figura, K., and Saftig, P. (1999). Targeted disruption of the lysosomal α-mannosidase gene results in mice resembling a mild form of human α-mannosidosis. Hum. Mol. Genet. *8*, 1365–1372.

15. Hubel, D.H., and Wiesel, T.N. (1998). Early Exploration of the Visual Cortex. Neuron *20*, 401–412.

16. Cummings, J.F., Wood, P.A., de Lahunta, A., Walkley, S.U., and Le Boeuf, L. (1988). The Clinical and Pathologic Heterogeneity of Feline Alpha-Mannosidosis. J. Vet. Intern. Med. *2*, 163–170.

17. Walkley, S.U., Thrall, M.A., Dobrenis, K., Huang, M., March, P.A., Siegel, D.A., and Wurzelmann, S. (1994). Bone marrow transplantation corrects the enzyme defect in neurons of the central nervous system in a lysosomal storage disease. Proc. Natl. Acad. Sci. USA *91*, 2970–2974.

18. Vite, C.H., McGowan, J.C., Niogi, S.N., Passini, M.A., Drobatz, K.J., Haskins, M.E., and Wolfe, J.H. (2005). Effective gene therapy for an inherited CNS disease in a large animal model. Ann. Neurol. *57*, 355–364.

19. Yoon, S.Y., Bagel, J.H., O'Donnell, P.A., Vite, C.H., and Wolfe, J.H. (2016). Clinical Improvement of Alpha-mannosidosis Cat Following a Single Cisterna Magna Infusion of AAV1. Mol. Ther. *24*, 26–33.

20. Yoon, S.Y., Hunter, J.E., Chawla, S., Clarke, D.L., Molony, C., O'Donnell, P.A., Bagel, J.H., Kumar, M., Poptani, H., Vite, C.H., and Wolfe, J.H. (2020). Global CNS correction in a large brain model of human alpha-mannosidosis by intravascular gene therapy. Brain *143*, 2058–2072.

21. Hunter, J.E., Molony, C.M., Bagel, J.H., O'Donnell, P.A., Kaler, S.G., and Wolfe, J.H. (2022). Transduction characteristics of alternative adeno-associated virus serotypes in the cat brain by intracisternal delivery. Mol. Ther. Methods Clin. Dev. *26*, 384–393.

22. Donsante, A., Yi, L., Zerfas, P.M., Brinster, L.R., Sullivan, P., Goldstein, D.S., Prohaska, J., Centeno, J.A., Rushing, E., and Kaler, S.G. (2011). ATP7A Gene Addition to the Choroid Plexus Results in Long-term Rescue of the Lethal Copper Transport Defect in a Menkes Disease Mouse Model. Mol. Ther. *19*, 2114–2123.

23. Vite, C.H., McGowan, J.C., Braund, K.G., Drobatz, K.J., Glickson, J.D., Wolfe, J.H., and Haskins, M.E. (2001). Histopathology, electrodiagnostic testing, and magnetic resonance imaging show significant peripheral and central nervous system myelin abnormalities in the cat model of alpha-mannosidosis. J. Neuropathol. Exp. Neurol. *60*, 817–828.

24. Kumar, M., Duda, J.T., Yoon, S.Y., Bagel, J., O'Donnell, P.A., Vite, C., Pickup, S., Gee, J.C., Wolfe, J.H., and Poptani, H. (2016). Diffusion Tensor Imaging for Assessing Brain Gray and White Matter Abnormalities in a Feline Model of α-Mannosidosis. J. Neuropathol. Exp. Neurol. *75*, 35–43.

25. Magnitsky, S., Vite, C.H., Delikatny, E.J., Pickup, S., Wehrli, S., Wolfe, J.H., and Poptani, H. (2010). Magnetic resonance spectroscopy of the occipital cortex and the cerebellar vermis distinguishes individual cats affected with alpha-mannosidosis from normal cats. NMR Biomed. *23*, 74–79.

26. Vite, C.H., Magnitsky, S., Aleman, D., O'Donnell, P., Cullen, K., Ding, W., Pickup, S., Wolfe, J.H., and Poptani, H. (2008). Apparent Diffusion Coefficient Reveals Gray and White Matter Disease, and T2 Mapping Detects White Matter Disease in the Brain in Feline Alpha-Mannosidosis. AJNR. Am. J. Neuroradiol. *29*, 308–313.

27. Katz, M.L., Tecedor, L., Chen, Y., Williamson, B.G., Lysenko, E., Wininger, F.A., Young, W.M., Johnson, G.C., Whiting, R.E.H., Coates, J.R., and Davidson, B.L. (2015). AAV gene transfer delays disease onset in a TPP1-deficient canine model of the late infantile form of Batten disease. Sci. Transl. Med. *7*, 313ra180.

28. Taghian, T., Marosfoi, M.G., Puri, A.S., Cataltepe, O.I., King, R.M., Diffie, E.B., Maguire, A.S., Martin, D.R., Fernau, D., Batista, A.R., et al. (2020). A safe and reliable technique for CNS delivery of AAV vectors in the cisterna magna. Mol. Ther. *28*, 411–421.

29. Taylor, R.M., and Wolfe, J.H. (1994). Cross-Correction of β-Glucuronidase Deficiency by Retroviral Vector-Mediated Gene Transfer. Exp. Cell Res. *214*, 606–613.

30. Wolfe, J.H., Sands, M.S., Harel, N., Weil, M.A., Parente, M.K., Polesky, A.C., Reilly, J.J., Hasson, C., Weimelt, S., and Haskins, M.E. (2000). Gene Transfer of Low Levels of β-Glucuronidase Corrects Hepatic Lysosomal Storage in a Large Animal Model of Mucopolysaccharidosis VII. Mol. Ther. *2*, 552–561.

31. Ertl, H.C.J. (2022). Immunogenicity and toxicity of AAV gene therapy. Front. Immunol. *13*, 975803.

32. Husain, T., Passini, M.A., Parente, M.K., Fraser, N.W., and Wolfe, J.H. (2009). Long-term AAV vector gene and protein expression in mouse brain from a small pancellular promoter is similar to neural cell promoters. Gene Ther. *16*, 927–932.

33. Watakabe, A., Ohtsuka, M., Kinoshita, M., Takaji, M., Isa, K., Mizukami, H., Ozawa, K., Isa, T., and Yamamori, T. (2015). Comparative analyses of adeno-associated viral vector serotypes 1, 2,5, 8 and 9 in marmoset, mouse and macaque cerebral cortex. Neurosci. Res. *93*, 144–157.

34. Hinderer, C., Katz, N., Buza, E.L., Dyer, C., Goode, T., Bell, P., Richman, L.K., and Wilson, J.M. (2018). Severe Toxicity in Nonhuman Primates and Piglets Following High-Dose Intravenous Administration of an Adeno-Associated Virus Vector Expressing Human SMN. Hum. Gene Ther. *29*, 285–298.

35. Hocquemiller, M., Giersch, L., Mei, X., Gross, A.L., Randle, A.N., Gray-Edwards, H.L., Hudson, J.A., Todeasa, S., Stoica, L., Martin, D.R., et al. (2022). AAVrh10 vector corrects pathology in animal models of GM1 gangliosidosis and achieves widespread distribution in the CNS of nonhuman primates. Mol. Ther. Methods Clin. Dev. *27*, 281–292.

36. Palazzi, X., Pardo, I.D., Sirivelu, M.P., Newman, L., Kumpf, S.W., Qian, J., Franks, T., Lopes, S., Liu, J., Monarski, L., et al. (2021). Biodistribution and Tolerability of AAV-PHP.B-CBh-SMN1 in Wistar an Rats and Cynomolgus Macaques Reveal Different Toxicologic Profiles. Hum. Gene Ther. *33*, 175–187.

37. Bolt, M.W., Brady, J.T., Whiteley, L.O., and Khan, K.N. (2021). Development challenges associated with rAAV-based gene therapies. J. Toxicol. Sci. *46*, 57–68.

38. Hordeaux, J., Buza, E.L., Dyer, C., Goode, T., Mitchell, T.W., Richman, L., Denton, N., Hinderer, C., Katz, N., Schmid, R., et al. (2020). Adeno-Associated Virus-Induced Dorsal Root Ganglion Pathology. Hum. Gene Ther. *31*, 808–818.

39. Buss, N., Lanigan, L., Zeller, J., Cissell, D., Metea, M., Adams, E., Higgins, M., Kim, K.H., Budzynski, E., Yang, L., et al. (2022). Characterization of AAV-mediated dorsal root ganglionopathy. Mol. Ther. Methods Clin. Dev. *24*, 342–354.

40. Cearley, C.N., Vandenberghe, L.H., Parente, M.K., Carnish, E.R., Wilson, J.M., and Wolfe, J.H. (2008). Expanded Repertoire of AAV Vector Serotypes Mediate Unique Patterns of Transduction in Mouse Brain. Mol. Ther. *16*, 1710–1718.

41. Cearley, C.N., and Wolfe, J.H. (2006). Transduction characteristics of adeno-associated virus vectors expressing cap serotypes 7, 8, 9, and Rh10 in the mouse brain. Mol. Ther. *13*, 528–537.

42. Cearley, C.N., and Wolfe, J.H. (2007). A Single Injection of an Adeno-Associated Virus Vector into Nuclei with Divergent Connections Results in Widespread Vector Distribution in the Brain and Global Correction of a Neurogenetic Disease. J. Neurosci. *27*, 9928–9940.

43. Lock, M., Alvira, M., Vandenberghe, L.H., Samanta, A., Toelen, J., Debyser, Z., and Wilson, J.M. (2010). Rapid, Simple, and Versatile Manufacturing of Recombinant Adeno-Associated Viral Vectors at Scale. Hum. Gene Ther. *21*, 1259–1271.